Investigation of momentum relaxation and time-dependent conductance in radiation-damaged GaAs

M. Haner
Department of Physics, University of California, Berkeley, California 94720

W. S. Warren
Department of Chemistry, Princeton University, Princeton, New Jersey 08544
(Received 8 September 1989)

We report experimental characterization of a transient capacitative electrical effect in a GaAs photoconductive switch due to initial momentum relaxation of the carriers within the photoexcited plasma. The carrier-momentum-dampening rate (τ_d) of approximately 1 ps is characterized by optical square-pulse excitation in a radiation-damaged GaAs substrate, which produces asymmetries in the electrical impulse response of the photoconductor. Defect densities in the radiation-damaged samples are measured with use of medium-energy Rutherford backscattering and correlated with the electrical characteristics. Simulations of the electron transport and electrical response under our experimental conditions agree favorably with the observed electrical characteristics of the photoconductor. We discuss the effect of plasma dampening on electrical-switching characteristics and the site-defect capture process.

I. INTRODUCTION

Electron transport in GaAs photoconductors is one of the most extensively studied phenomena in solid-state physics. Carrier relaxation and recombination dynamics in these devices are of fundamental importance to the development of high-speed GaAs optoelectronic circuits. As long as good Ohmic contact is established, the electrical characteristics or impulse response of the switch is determined by the temporal shape of the excitation laser pulse and the intrinsic carrier lifetime in the semiconductor.[1] This is valid only if the photoexcited electron-hole plasma is sufficiently dampened so that the momentum relaxation does not significantly affect the transport or conductivity in the semiconductor gap. If the plasma-dampening rate is comparable to the electrical response time of the switch, a time-dependent capacitance may be present which limits the electrical response of the photoconductor. This is especially important in photon-controlled millimeter-wave switches[2] and in dc-biased photoconductors where photoexcited carriers induce space-charge fields at deep-level trap sites in the semiconductor.[3] The transient nature of momentum relaxation in the electron plasma is a critical parameter in these photoconductive devices. In particular, if the electrical response is approximately limited by carrier transport, the macroscopic effect of a time-varying gap capacitance warrants further investigation.

In this paper we present measurements which illustrate the effect of momentum relaxation of the photoexcited carriers on the electrical rise and fall times of the GaAs photoconductive switch. The plasma-dampening rate of the photoexcited carriers in the radiation-damaged semiconductor is comparable to the electrical response of the switch. These measurements are made on a coplanar photoconductive switch fabricated with radiation-damaged GaAs. Our experimental studies are facilitated by our laser system, which allows us to synthesize rectangular optical excitation pulses with rise and fall times of ≤ 100 fs and arbitrary temporal lengths. The optical pulses act as optical step functions which allow some of the electron-hole–relaxation mechanisms to equilibrate before the excitation is essentially "turned off." By systematically lengthening the rectangular pulses used to excite the photoconductor, we can indirectly probe transient carrier relaxation on the order of 1 ps, which contributes to capacitative effects and electrical responsivity of the photoconductor. Our results indicate a possible way to compensate for some plasma-relaxation artifacts in the photoconductor response which lead to electrical-impulse asymmetries and other experiments which may be useful in understanding the phenomena. The radiation damage in the samples significantly affects the plasma dynamics and recombination of carriers in the semiconductor. The fundamental aspects of the correlation between trap sites and electrical response is of practical importance in incorporating photoconductive and electronic devices, such as field-effect transistors (FET's), into integrated optoelectronic circuits.[4]

II. EXPERIMENTAL MEASUREMENTS

High-resistivity epitaxial GaAs photoconductors were fabricated by molecular-beam epitaxy (MBE) on a 60-μm, semi-insulating, undoped GaAs substrate thermostatted to 600 °C. A 30-μm epitaxial layer of GaAs was grown on the substrate at a growth rate of 1.5–2.0 μm/h. The capacitance-voltage profiles and resistivity measurements of the epitaxial substrate showed an intrinsic carrier density of 3.5×10^{16} cm^{-3} and a dark resistance of 2.0×10^{8} Ω. The GaAs substrates were radiation damaged with

50-keV, 300-keV, and 2-MeV protons at a fluence of $\approx 1.0\times10^{14}$ cm^{-3}. Defect-density profiles were then determined by Rutherford backscattering [Fig. 1(a)] under ultrahigh vacuum (2.0×10^{-8} Torr). These measurements were calibrated by comparison with single-crystal (100) GaAs samples cut and oriented to $\pm0.5°$ and amorphous GaAs samples. A toroidal-type electrostatic analyzer was used with energy and depth resolution of 1×10^{-3} and 0.5–0.6 nm, respectively. Defect densities [Fig. 1(b)] ranged from approximately 10^{12} to 10^{13} cm^{-3} in the radiation-damaged samples. Note that changing the ^{4}He kinetic energy changes the defect depth, but not the surface defect density.

A coplanar photoconductor (Fig. 2), with 25-μm conduction and sampling gaps and 15-μm$\times$2.5-cm transmission lines, was fabricated on the GaAs substrates using a photolithographic liftoff technique. A layered metallization consisting of Ge(500 Å)/Ni(100 Å)/Au(1000 Å)/Ti(500 Å)/Au(2000 Å) was deposited on to the masked surface using an electron-beam evaporator. Additional contact pads were defined on the surface for measurement of contact resistances for the transmission lines. The metallized lines and pads were alloyed in an AG Associates halogen-lamp annealing station under continuous dry-N_2 flow. The wafer was initially heated to 375° C for 10–15 s at a heating rate of 50° C/s with an additional heating cycle to 490 °C for 10 s to complete the alloying process. The substrate and metallized lines were examined under a scanning electron microscope (SEM) to determine the uniformity of the alloying procedure and the edge morphology in the photoconductor gaps. A contact resistance of 4.5×10^{-6} Ω cm^2 was achieved using the alloyed metallization scheme.

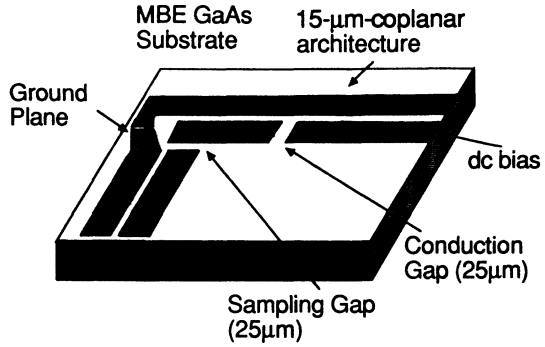

FIG. 2. Photoconductive architecture used for our experimental measurements. The device was fabricated by a standard liftoff technique on radiation-damaged GaAs. The propagation length between the 25-μm sampling and conduction gaps is 0.1 mm.

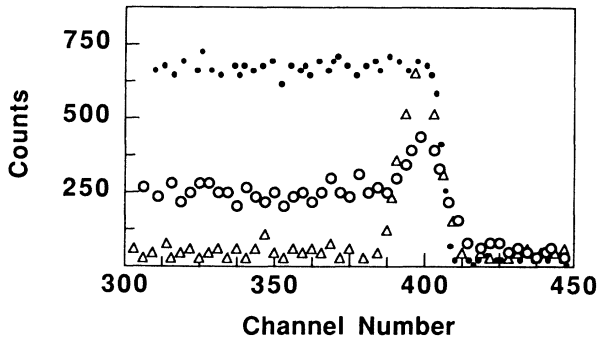

(a)

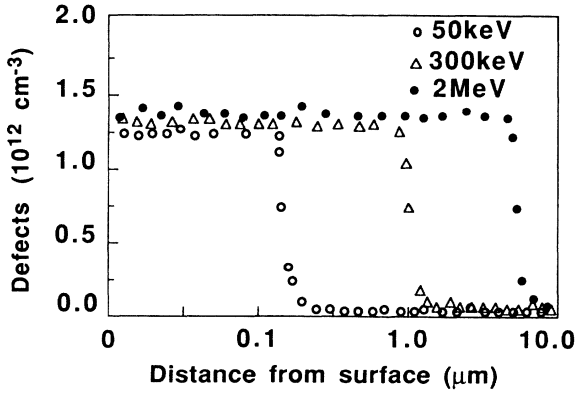

(b)

FIG. 1. (a) Experimental Rutherford backscattering spectra for samples of amorphous GaAs (solid circles), radiation-damaged GaAs (2-MeV ^{4}He, open circles), and single-crystal GaAs (triangles, 100). Spectra were taken at 2.3 keV/channel. (b) Defect densities as a function of ^{4}He kinetic energy.

Rectangular optical pulses illustrated in Fig. 3 with

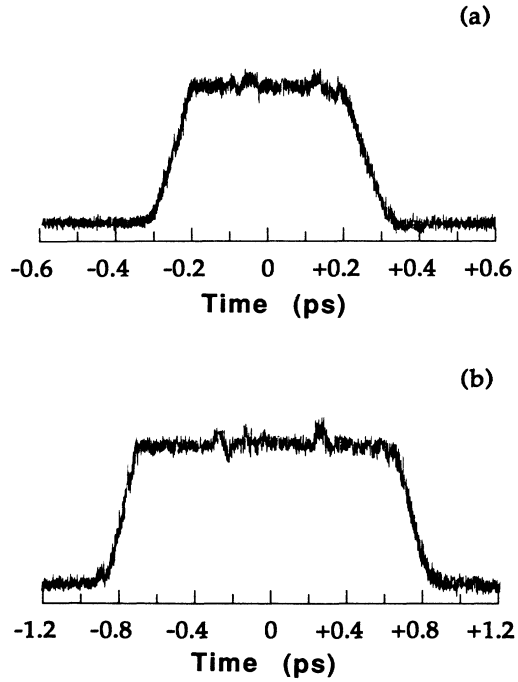

FIG. 3. Experimental cross-correlation traces of two of the optical excitation pulses (corresponding to 0.6- and 1.2-ps duration) used in this experiment. In each case the pulse was cross correlated with a 180-fs sech^2 pulse, which has been deconvolved from the data. The pulse length was varied to systematically probe the transient electrical response of the photoconductor.

rise times of ≈90 fs and sequentially increasing lengths from 0.5 to 1.5 ps were synthesized by time-domain modulation in a fiber-gating compressor combined with chirped pulse amplification.[5] The temporal shape, widths, and rise times of the pulses were verified by cross correlation with a 180-fs sech^2 pulse and by measurement of the spectral bandwidth of the pulses. The rise and fall times of the pulses were consistently 90–100 fs with 2–3% uniformity over the central region. Excitation pulses at $\lambda=0.65$ μm (1.90 eV) were spatially filtered, attenuated with two crossed polarizers, and focused to a spot size of approximately 100 μm^2 onto the photoconductive gap. To calibrate the photoconductor, the 180-fs sech^2 pulse was used to excite both the conducting and sampling gaps [Fig. 4(a)] with resulting rise and fall times of 2.5 and 4.4 ps, respectively. The average photocurrent was measured at the sampling gap (with a current-voltage converter and lock-in amplifier at a 1-kHz sampling rate) as a function of the time delay between the conducting and sampling optical pulses.

Rectangular laser pulses with five different durations from 0.6 to 1.65 ps were then used to excite the photoconductor gap; the 180-fs sech^2 pulse still illuminated the sampling gap. The intensity of the rectangular pulses was adjusted to maintain a constant carrier density of approximately 3.0×10^{17} cm^{-3}. The average photocurrent measured at the sampling gap, shown in Figs. 4(b)–4(d) and summarized in Table I, provides a cross-correlation of the electrical-impulse response of the photoconductor. All measured rise times are comparable (2.4–2.6 ps). However, the most important feature observed upon excitation with the 0.6- and 0.78-ps rectangular pulses is the asymmetric 4.4–4.6-ps fall time. This asymmetry is absent from the response measured with the 1.3-ps rectangular excitation pulse which yields nearly symmetric 2.5- and 2.8-ps rise and fall times. The electrical responses are *independent* of the ^{4}He bombardment energy. This implies that the asymmetry arises predominantly from a surface effect; if bulk phenomena were involved, Fig. 1(b) implies that some bombardment-energy dependence would have been observed.

TABLE I. Measured electrical rise and fall times for the radiation-damaged GaAs photoconductor as a function of the temporal width of the excitation pulse. The deconvolution error in rise and fall times is ±0.3 ps. Sequentially lengthening the pulse width lets the photoexcited plasma undergo a finite time evolution, and systematically decreases the fall time. (rect. denotes rectangular.)

Optical pulse	τ_{rise} (ps)	τ_{fall} (ps)	ρ (10^{17} cm^{-3})
0.18 ps sech^2	2.5	4.4	2.5
0.60 ps rect.	2.4	4.6	2.8
0.78 ps rect.	2.6	4.1	3.0
0.89 ps rect.	2.6	3.7	3.0
1.30 ps rect.	2.5	2.8	2.7
1.65 ps rect.	2.7	2.6	2.3

The origin of this rise-fall–response difference was not readily discernible from the photocurrent-decay data and was evaluated further by stimulating the photoconductor response under the conditions used in our experiment. We determined that the observed transient effect could not be attributed to the high-frequency properties of the coplanar microstrip by calculating the propagating-mode structure and dispersion (1 GHz–1 THz) of the transmission lines in our photoconductor.[6] A fast-Fourier-transform (FFT) algorithm was used to calculate both TE and TM-mode propagation along the microstrip,

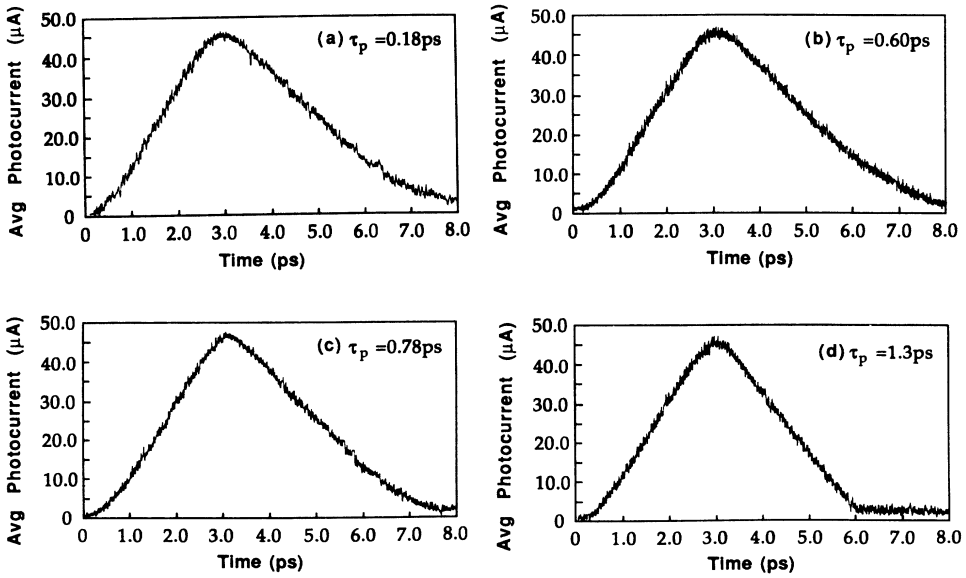

FIG. 4. Experimental photocurrent transient data are shown using excitation pulses of (a) 0.18 ps, (b) 0.6 ps, (c) 0.78 ps, and (d) 1.3 ps. All pulses have ≈90-fs rise and fall times, comparable to Fig. 3. The optical intensity was adjusted to maintain a carrier density of ≈3.0×10^{17} cm^3. Note the disappearance of asymmetry in the response as the pulse length increases.

frequency-dependent phase velocity, electrical loss, and a propagation constant, β_{TEM}.[7] The electrical-pulse shape was calculated at 50-μm intervals along the microstrip to a total length of 2.0 mm to simulate propagation of the picosecond photoconductive pulse. The simulation results indicate a quasi-TEM propagating mode in the coplanar transmission line with nearly square-root-dependent electrical loss. The simulated electrical-pulse shape does undergo significant broadening at lengths of 1–2 mm; however, the high-frequency dispersion associated with the microstrip does not account for the observed transient asymmetry, as there was essentially no difference in the propagating-mode structure or dispersion calculated for all three rectangular optical pulses used for excitation.

The asymmetry in the photocurrent decay as a function of excitation-pulse width underlies a finite equilibration time in the photoexcited plasma comparable to the conduction response for the photoconductor (roughly 1 ps). If we examine the photoconductor as a lumped-element circuit,[1,8] the asymmetric settling time (4.5 ps) corresponds to a transient gap capacitance of approximately 0.4 fF.

III. ANALYSIS OF ELECTRON TRANSPORT

Photoelectron dynamics corresponding to different experimental conditions in the planar GaAs switch can be modeled using Monte Carlo methods to simulate carrier transport.[9] In particular, initial carrier distributions in momentum space ($\mathbf{k}\cdot\mathbf{p}$) can be calculated. Macroscopic ensemble averages must be consistent with Maxwell's equations, the rate equations for defect trapping, Poisson's equation convection, and must also reproduce Ohm's law.[10] The action of an externally applied electric field gradient is included in the computation for drift and diffusion through Einstein's relation for the electron or hole mobility [$D_{n,p}=(kT/q)\mu_{n,p}$]. The computation scheme consists of an energy distribution of nonrelativistic electrons and holes in a given volume surrounding some position r in the semiconductor at time t. The ith electron or hole in the ensemble has position $\mathbf{r}_i(t)$ and velocity $\mathbf{v}_i(t)$ and contributes to the macroscopic properties of the photoconductor at position r through a weighting function $w_i(\mathbf{r},t)$. The magnitude of $w_i(\mathbf{r},t)$ is proportional to $\mathbf{r}-\mathbf{r}_i(t)$. The accumulated charge, current density, electron pressure, and resistivity tensors are defined by, respectively,

$$q(\mathbf{r},t)\equiv -e\sum_i w_i(\mathbf{r},t)\ , \tag{1}$$

$$\mathbf{j}(\mathbf{r},t)\equiv -e\sum_i \mathbf{v}_i w_i(\mathbf{r},t)\ , \tag{2}$$

$$\mathbf{P}(\mathbf{r},t)\equiv m\sum_i \mathbf{v}_i\mathbf{v}_i w_i(\mathbf{r},t)\ , \tag{3}$$

$$\eta\mathbf{j}(r,t)\equiv -e\sum_i (\dot{\Gamma}_i+\dot{N}_i)\mathbf{v}_i w_i(\mathbf{r},t)\ . \tag{4}$$

In $\mathbf{k}$ space the ensemble changes continuously over a period of time t; therefore the distribution function $\langle S\rangle = c\sum n(\mathbf{k})s(\mathbf{k})$ is found within a given discrete value of $\Delta\mathbf{k}$. Macroscopic values for electron-electron, electron-phonon (polar optical and acoustic), electron-defect, and intervalley scattering are obtained by statistically calculating the distribution function before and after a given number of scattering events. The time-varying aggregate densities of electrons and holes can be written as

$$\partial n/\partial t=\gamma(\mathbf{r},t)-T_n(\mathbf{r},t)+(1/q)\nabla\cdot\mathbf{J}_n\ , \tag{5}$$

$$\partial p/\partial t=\gamma(\mathbf{r},t)-T_p(\mathbf{r},t)+(1/q)\nabla\cdot\mathbf{J}_p\ , \tag{6}$$

where $n(\mathbf{r},t)$ and $p(\mathbf{r},t)$ are the electron or hole densities, $\gamma(\mathbf{r},t)$ is the electron-hole–pair photogeneration rate, $T_n(\mathbf{r},t)$ and $T_p(\mathbf{r},t)$ are the trapping rates, q is the electronic charge, and $\mathbf{J}_n(\mathbf{x},t)$ and $\mathbf{J}_p(\mathbf{x},t)$ are the current densities.[9,11] The total current density [Eq. (2)] is then equal to $\mathbf{J}_n(\mathbf{x},t)+\mathbf{J}_p(\mathbf{x},t)+\mathbf{J}_d(\mathbf{x},t)$, where $\mathbf{J}_d(\mathbf{x},t)$ is the displacement current ($\epsilon\,\partial\mathbf{E}/\partial t$). The expressions for $\mathbf{J}_n(\mathbf{x},t)$ and $\mathbf{J}_p(\mathbf{x},t)$ are given by

$$\mathbf{J}_n(\mathbf{x},t)=q(\mu_n\mathbf{E}n+D_n\nabla n)\ , \tag{7}$$

$$\mathbf{J}_p(\mathbf{x},t)=q(\mu_p\mathbf{E}n-D_p\nabla p)\ . \tag{8}$$

Poisson's equation couples the transport dynamics of the photoexcited carriers through the drift contribution in the current-density equation. It is generally written as

$$\nabla^2\Omega=-\nabla\cdot\mathbf{E}=-q/\epsilon(p-n-n_T^-)\ , \tag{9}$$

where Ω is the electric potential and ϵ is the static dielectric constant.

The carrier-trapping rates for electrons and holes is proportional to the free-carrier density and the number of available trap sites in the semiconductor. The carrier-trapping rates are given by

$$T_n(\mathbf{r},t)=\langle\mathbf{v}_n\rangle\beta_n(nn_T^0) \tag{10}$$

and

$$T_p(\mathbf{r},t)=\langle\mathbf{v}_p\rangle\beta_p(n_T^-)\ , \tag{11}$$

where $\mathbf{v}_n$ and $\mathbf{v}_p$ are the electron and hole thermal velocities, and β_n and β_p are the electron and hole capture cross sections.[12] The total number of trap sites is given by $N_T=n_T^0+n_T^-$, where n_T^0 and n_T^- are the total neutral and negatively charged trap sites in the semiconductor.

The macroscopic equations are then written in terms of the change in electrons, holes, and available trap sites from thermal equilibrium after excitation with the laser pulse. Using detailed balance and charge neutrality, Eqs. (7)–(11) can be rewritten into a system of four differential equations in one spatial dimension, which can be used to numerically describe the photoconductor response,[9,12]

$$\partial \Delta n/\partial t = \gamma(r,t) - \beta_n(N_T - n_T^- - \Delta n_T^-)\Delta n + \mu_n\{[\partial(E\,\Delta n)/\partial x] + (kT/q)(\partial^2 \Delta n/\partial x^2)\}\ , \tag{12}$$

$$\partial \Delta p/\partial t = \gamma(r,t) - \beta_p(n_T^- - \Delta n_T^-)\Delta p + \mu_p\{[-\partial(E\,\Delta p)/\partial x] + (kT/q)(\partial^2 \Delta p/\partial x^2)\}\ , \tag{13}$$

$$\partial \Delta n_T^-/\partial t = \beta_n(N_T - n_T^- - \Delta n_T^-)\Delta n - \beta_p(n_T^- - \Delta n_T^-)\Delta p\ , \tag{14}$$

$$\partial^2 \Omega/\partial x^2 = -\partial E/\partial x = -(q/\epsilon)(\Delta p - \Delta n - \Delta n_T^-)\ . \tag{15}$$

To complete the mathematical description of our photoconductor, we must include the appropriate boundary-value problems; the electrical contacts are defined at $x=0$ and L and the contact at $x=0$ is chosen to have the electric field reference $(+V_0)$. The initial field quantities are given by $\Omega(0,t)=0$, $\Omega(L,t)=-V_0$, $\Omega(x,0)=-V_0(x/L)$, and $E(x,0)=V_0/L$.

Equations (12)–(15) constitute a standard set of nonlinear differential equations which can be numerically solved using a variety of techniques. The following results were obtained using a spatially discrete finite-element method which can be integrated for arbitrary response time.[13] Computed electrical responses for the GaAs photoconductor were performed as a function of excitation pulse shape, duration, and rise and fall time, and the applied bias voltage with a constant gap spacing. Electric field contours were digitally represented for our specific device geometry rather than using a spatially uniform field. For a given optical field, the allowed transitions from the heavy-hole, light-hole, and split-off bands result in three distinct **k**-space levels for the excited electrons in the conduction bands. Scattering parameters used in the simulation included electron-phonon, electron-electron, electron-hole, and intervalley scattering ($\Gamma \rightarrow L$, $\Gamma \rightarrow X$).[10] The characteristics relevant to our experimental data include energy relaxation, Ohmic mobility, drift velocity, diffusion, and thermalization rate. The macroscopic time-dependent electrical characteristics of the photoconductor can be simulated by incorporating the electron dynamics into the coupled partial-differential transmission-line equations. Computed electrical responses for the GaAs photoconductor were performed as a function of excitation-pulse shape, duration, and rise and fall time, and the applied bias voltage with a constant gap spacing. Simulation parameters are listed in Table II. Values for free-carrier scattering, thermalization ($\tau \approx 200$ fs), and intervalley transfer rates were also calculated and are consistent with previously reported results.[11,12]

Figure 5 shows the calculated average electron velocity versus time at static fields of 1, 5, and 10 kV/cm, with the corresponding transient velocity responses ($1/e$) being 0.7, 0.5, and 0.4 ps, respectively. Velocity overshoot was not predicted in the simulation results or observed experimentally for excitation at 1.9 eV at bias fields up to 10 kV. The average electron energy, at 1.9 eV excitation, is greater than the minimum L-valley energy, and as a result very rapid $\Gamma \rightarrow L$ transfer reduces the possible effects of velocity overshoot. Figure 6 shows the calculated average electron momentum after excitation. The pho-

TABLE II. Coefficients and parameters used in the Monte Carlo calculation, exclusive of the photoconductor boundary conditions.

Parameters	
Density (g/cm^3)	5.37
Energy-band gap (eV)	1.43
Optical excitation energy (eV)	1.90
Plasma carrier density (cm^3)	2.5×10^{17}
high-frequency dielectric constant	10.90
Static dielectric constant	12.85
Ballistic speed of sound (cm/s)	5.22×10^5
Lattice constant (cm)	5.64×10^{-8}

	Γ valley	L valley	X valley
Effective-mass ratio	0.063	0.226	0.576
Number of equivalent valleys	1	4	3
Valley separation (eV) from Γ valley		0.30	0.53
Nonparabolicity factor (eV^{-1})	0.62	0.43	0.22
Polar optical-phonon energy (eV)	0.036	0.036	0.036
Acoustic deformation potential (eV)	6.78	6.45	5.98

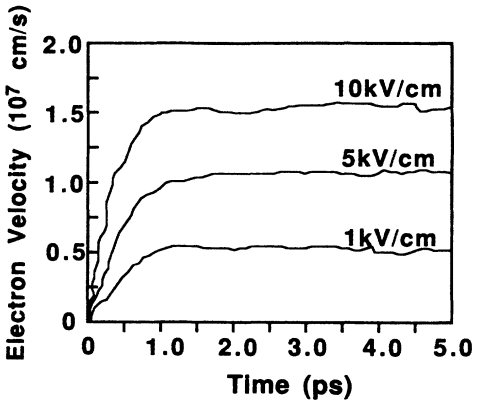

FIG. 5. Calculated average electron velocity as a function of bias voltage. At an excitation energy of 1.90 eV, no velocity overshoot was observed in the simulations.

toexcited plasma undergoes an initial relaxation decay which approaches a steady-state value at roughly 2 ps. These transient data provide a plasma-dampening rate (τ_d) of approximately 1 ps, which can then be incorporated into the differential equations used to calculate the electrical response of the photoconductor. The traces shown in Fig. 7 illustrate the calculated electrical responses for our GaAs photoconductor under experimental conditions assuming $\tau_d \ll \tau_r$ [Fig. 7(a)] and $\tau_d \approx \tau_r$ [Fig. 7(b)]. The calculation was performed using a split-energy-level recombination model at the trap centers in the bulk semiconductor.[14] The computed responses with $\tau_d \approx \tau_r$ agree fairly well with the experimental data; the corresponding calculated rise and fall times for excitation-pulse widths ≤ 1 ps are 2.25 and 4.25 ps, respectively. Recombination phenomena at trap sites in Fe:InP have also been shown to produce asymmetric photoconductive responses in these devices.[3]

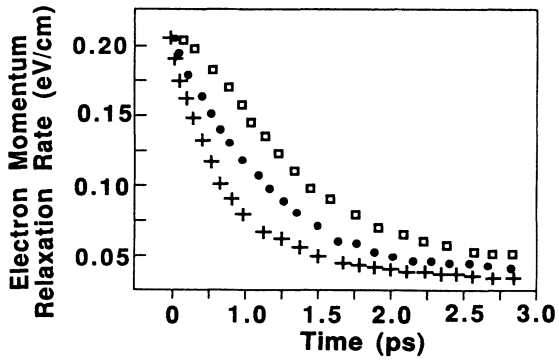

FIG. 6. Calculated momentum-relaxation rate of the photoexcited plasma; the decay data provide a plasma dampening rate (τ_d) of approximately 1 ps. Squares are 50 keV, solid circles 300 keV, and crosses 2 MeV proton energies; also shown are the corresponding defect densities produced.

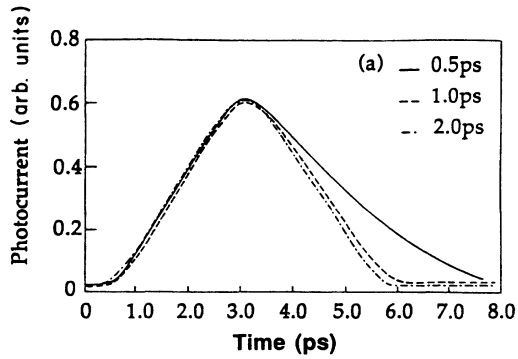

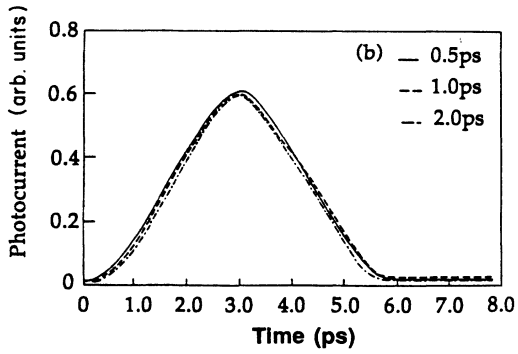

FIG. 7. Calculated electrical responses for our GaAs photoconductor assuming a plasma dampening of (a) $\tau_d = 1$ or assuming (b) $\tau_d \ll \tau_r$ for rectangular 0.5-, 1.0-, and 2.0-ps excitation pulses. Rise times for all three pulse durations were consistently about 2 ps; however, the fall times vary from 2 to 5 ps.

IV. DISCUSSION AND SUMMARY

The effect of this transient capacitance may be most pronounced in devices which have response times (≈ 1 ps) limited principally by the carrier transport in the semiconductor. It may also be important in millimeter-wave applications where transient capacitance would impair the response time and degrade the switching efficiency of the photoconductor. The measurements reported here using variable-length rectangular pulses allows one to indirectly observe electron transport in photoexcited plasma and to correlate this with electrical properties of the photoconductor. It also points to a possible utility of pulse synthesis in measuring other time-dependent artifacts in photoconductive circuits. Rectangular pulses may be synthesized with fast rise times (≈ 90 fs) and a duration which can be sufficiently long to allow the photoexcited plasma to reach a steady state. This technique provides a new time-resolved measurement to be made in photoconductive devices.

In summary, the defect-density profile in a radiation-damaged GaAs photoconductor was correlated with the observed electrical transient response of the photoconductor. Experimental photocurrent transient data show a correlation between the rise and fall response and the excitation-pulse width, which is attributed to a time-varying capacitance in the photoconductor. The relaxa-

tion rate was determined to be ≈ 1 ps by excitation with rectangular ($\tau_r \leq 100$ fs) optical pulses with variable durations. Simulation results indicate that the photoexcited carriers undergo an initial momentum relaxation due to insufficient plasma dampening, and that the dampening artifact is due to recombination at the intrinsic trap sites which produces a time-varying capacitance in the photoconductor. Simulations with a plasma-dampening rate of 1 ps reproduce the observed transient response fairly accurately, while similar calculations, including space-charge generation at trap sites, are inconclusive.

ACKNOWLEDGMENTS

This work was supported by the U.S. National Science Foundation (NSF) under Grant No. CHE-87-19545 and by the U.S. Defense Advanced Research Projects Agency (DARPA) under Contracts No. N60921-87-C-0023 and No. N60921-88-C-0273, administered by the U.S. Naval Surface Warfare Center (NSWC). One of us (M.H.) would also like to thank the Miller Institute for Basic Research in Science at the University of California for support.

[1]D. H. Auston, IEEE J. Quantum Electron. **QE-19**, 639 (1983); A. M. Johnson, R. M. Lum, W. M. Simpson, and J. Klingert, *ibid.* **QE-23**, 1180 (1987).

[2]A. M. Vaucher, C. D. Striffler, and C. H. Lee, IEEE Trans. Microwave Theory **MTT-31**, 209 (1983); W. Platte, *ibid.* **MTT-29**, 1010 (1981).

[3]B. Hwang, F. A. Lindholm, and R. B. Hammond, IEEE J. Quantum Electron. **QE-19**, 648 (1983).

[4]K. J. Weingarten, M. J. W. Rodwell, and D. M. Bloom, IEEE J. Quantum Electron. **QE-24**, 198 (1988).

[5]M. Haner and W. S. Warren, Appl. Phys. Lett. **52**, 1458 (1988); M. Haner and W. S. Warren, in *Ultrafast Phenomena IV,* edited by C. B. Harris and T. Yajima (Springer-Verlag, Berlin, 1988).

[8]R. B. Hammond, N. G. Paulter, and R. S. Wagner, Appl. Phys. Lett. **45**, 289 (1984).

[7]R. E. Collin, *Field Theory of Guided Waves* (McGraw-Hill, New York, 1960).

[8]K. K. Li, G. Arjavalingam, A. Dienes, and J. R. Whinnery, IEEE Trans. Microwave Theor. Tech. **MTT-30**, 1270 (1982).

[9]A. E. Iverson and D. L. Smith, IEEE Trans. Electron Dev. **ED-34**, 2098 (1987).

[10]M. A. Osman and D. K. Ferry, J. Appl. Phys. **61**, 5330 (1987); C. Jacoboni and L. Reggiani, Rev. Mod. Phys. **55**, 645 (1983).

[11]A. J. Taylor, D. J. Erskine, and C. L. Tang, J. Opt. Soc. Am. Ser. B **2**, 663 (1985).

[12]P. Lugli and D. K. Ferry, Physica B+C (Amsterdam) **134B**, 369 (1985); K. Seeger, *Semiconductor Physics* (Springer-Verlag, Berlin, 1982); H. U. Barager and J. W. Wilkins, Phys. Rev. B **30**, 7349 (1984).

[13]L. Reggiani, in *High Field Electron Transport* (Springer-Verlag, Berlin, 1985); B.-K. Hu and J. W. Wilkins, Phys. Rev. B **39**, 8464 (1989).

[14]G. K. Wertheim, Phys. Rev. **109**, 1086 (1958).

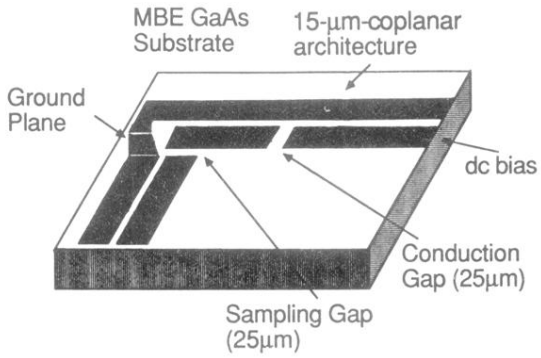

FIG. 2. Photoconductive architecture used for our experimental measurements. The device was fabricated by a standard liftoff technique on radiation-damaged GaAs. The propagation length between the 25-μm sampling and conduction gaps is 0.1 mm.